Electrically-tunable pore morphology in nanoporous gold thin films

Article *in* Nano Research · April 2015

Impact Factor: 7.01 · DOI: 10.1007/s12274-015-0726-x

2 authors, including:

Erkin Seker
University of California, Davis
60 PUBLICATIONS **474** CITATIONS

Nano Research
DOI 10.1007/s12274-015-0726-x
Research Article
ISSN 1998-0124
CN 11-5974/O4

Electrically-tunable pore morphology in nanoporous gold thin films

Tatiana S. Dorofeeva[1], and Erkin Seker[1](✉)

Nano Res., **Just Accepted Manuscript** • DOI 10.1007/s12274-015-0726-x
http://www.thenanoresearch.com on January 28, 2015

Just Accepted

TSINGHUA UNIVERSITY PRESS Springer

Template for Preparation of Manuscripts for *Nano Research*

TABLE OF CONTENTS (TOC)

Electrically-Tunable Pore Morphology in Nanoporous Gold Thin Films Tatiana S. Dorofeeva, Erkin Seker * University of California – Davis, USA	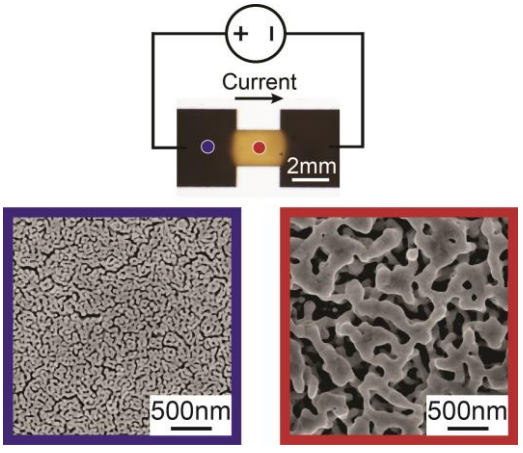 Electrical current is used for tuning pore morphology of nanoporous gold thin films at significantly lower temperatures than previously reported via electrically-assisted mechanisms. This technique allows for precisely controlling the extent and location of pore coarsening and producing a wide range of distinct morphologies on a single substrate for high-throughput studies of structure-property relationships.

Erkin Seker, http://web.ece.ucdavis.edu/~eseker/index.html

Nano Research
DOI (automatically inserted by the publisher)
Research Article
ISSN 1998-0124
CN 11-5974/O4

Electrically-tunable pore morphology in nanoporous gold thin films

Tatiana S. Dorofeeva[1], and Erkin Seker[1](✉)

[1] *Department of Electrical and Computer Engineering, University of California – Davis, Davis, CA 95616, USA*

Received: day month year
Revised: day month year
Accepted: day month year (automatically inserted by the publisher)

KEYWORDS

nanoporous gold,
tunable morphology,
Joule heating,
material screening

ABSTRACT

Nanoporous gold (np-Au) is an emerging nanostructured material that exhibits many desirable properties, including high electrical and thermal conductivity, high surface area-to-volume ratio, tunable pore morphology, well-established surface-binding chemistry, and compatibility with microfabrication. These features made np-Au a popular material for fuel cells, optical and electrical biosensors, drug delivery vehicles, neural electrode coatings, and as a model system for nano-scale mechanics. In each application, np-Au morphology plays an essential role in the overall device operation. Therefore, precise control of morphology is necessary for attaining optimal device performance. Traditionally, thermal treatment in furnaces and on hot plates is used for obtaining np-Au with self-similar but coarser morphologies. However, this approach lacks the ability to create different morphologies on a single substrate and requires high temperatures (>250 °C) that are not compatible with most plastic substrates. Herein, we report electro-annealing as a method that for the first time makes it possible to control the extent and location of pore coarsening on a single substrate with one fast treatment step. In addition, the electro-annealing entails much lower temperatures (<150 °C) than traditional thermal treatment, putatively due to electrically-assisted phenomena that contribute to thermally-activated surface diffusion of gold atoms responsible for coarsening. Overall, this approach can be easily scaled up to display multiple pore morphologies on a single chip and therefore enable high-throughput screening of optimal nanostructures for specific applications.

1. Introduction

Nanostructured materials have attracted significant interest from academia and industry alike, due to intriguing fundamental questions around nanoscale phenomena and applications enabled by properties unique to this length scale. Optical, electrical, magnetic, thermal, mechanical properties become

Address correspondence to Erkin Seker, eseker@ucdavis.edu

increasingly size-dependent at nanoscale [1]. Nanostructured materials have been shown to exhibit high strength [2], unusual thermal and electrical properties [3, 4], and enhanced surface plasmons [5], highlighting the importance of controlling nanostructure. An emerging nanostructured material is nanoporous gold (np-Au), for which related applications and publications have rapidly grown during last decade [6]. This popularity is due to many of its attractive properties, including high electrical and thermal conductivity, high surface area-to-volume ratio, tunable pore morphology, well-established gold binding chemistry, and compatibility with microfabrication [6]. These properties had an impact on applications including sensing [7, 8]. biomedical devices [9-12], energy storage [13], photonics [14, 15], catalysis [16, 17], as well as fundamental structure-property studies [18-21].

Nanoporous gold is typically obtained by a process known as *dealloying* [22]. In this process, selective removal of silver atoms from a silver-rich gold alloy, accompanied by surface diffusion of gold atoms at the metal-electrolyte interface, results in an open-cell structure with interconnected ligaments of tens of nanometers [22, 23]. Alloy composition [24] and preparation approach, dealloying method [25-27], and post-processing techniques [28, 29] all influence pore morphology, resulting in a wide range of possible pore and ligament sizes ranging from tens of nanometers [25] up to several hundred of nanometers [23]. When np-Au films are subjected to homogenous thermal treatment (such as in annealing furnaces), pore and ligament sizes increase in a uniform fashion across the entire sample due to enhanced diffusion of surface atoms [23]. However, a controllable spatial gradient of pore morphology is highly desirable in order to rapidly identify optimal morphologies for desired application [29]. For example, it is often necessary to identify a specific range of nanostructures that increase surface-enhanced Raman signal from a metallic surface, improve biocompatibility, lower limit-of-detection of a sensor, or increase reactivity of a catalytic surface. With the uniform exposure to thermal energy in conventional annealing approaches, it is not possible to obtain different pore morphologies on a single substrate. In addition, traditional thermal treatment in furnaces or on hot plates requires temperatures of at least 250 °C [23]; thereby, rendering this technique incompatible with most plastic substrates with low melting temperatures [30].

Here, we present a novel technique to address these challenges by taking advantage of the electrical conductivity of np-Au thin films in order to tune pore morphology. Specifically, we employ *electro-annealing* of micropatterned np-Au thin film patterns with rationally-designed geometries to obtain distinct pore morphologies on a single chip. This technique is based on the principle that electrical current flowing in thin film traces lead to localized changes in current density as a function of trace geometry. At regions with smaller cross-section, increased current density leads to localized Joule heating (also known as ohmic and resistive heating) and putatively enhances *electrically-assisted* coarsening mechanisms (to be discussed in section 3.4). The interplay of thermal and electrical mechanisms consequently produces coarsened morphologies at temperatures much lower (~150 °C) than those required for pure thermal annealing [23], thus opening the door to the use of substrates with lower melting temperatures. In tandem, this method, for the first time, allows for creating multiple and distinct pore morphologies on a single substrate via a short (less than 2 minutes), single treatment step. Here, we describe the electro-annealing technique and illustrate resultant pore morphologies. Finally, a comparative study on differences between temperature and morphology for electro- and hot plate-annealing approaches is presented. We expect that this novel approach will facilitate the production of

high-throughput screening platforms on various substrates for studying structure-property relationships and identifying optimal morphologies for desired applications.

2. Experimental

In order to study the effect of thin film geometry on pore morphology evolution, we fabricated samples with various np-Au thin film patterns on glass coverslips: (i) simple rectangular traces, referred to as *unconstricted* samples (Figure 1A); (ii) geometric variations that act as electrical current concentrators within the rectangular traces, referred to as *constricted* samples (Figure 3A); and (iii) branched trace structures with constrictions that act as current dividers controlling the extent of electro-annealing (Figure 4A). The np-Au traces (460 nm-thick) on glass coverslips were produced by dealloying lithographically-patterned gold-silver thin films that were sputter-deposited, as previously described [31]. The prepared samples were mounted on a homemade electro-annealing test fixture (Figure S-1 in the ESM), constant current was injected into the trace through the clips, and the sample temperature was measured by an infrared (IR) thermometer positioned over the sample (Figure S-2 in the ESM). High-magnification sample images were obtained with a scanning electron microscope (SEM) and the median ligament thicknesses were extracted from each image to quantify morphology evolution.

Chemicals and Materials: Glass coverslips (24 x 60 mm, thickness 0.13 - 0.16 mm) were purchased from Fisher Scientific. Piranha solution, used for cleaning the coverslips, consisted of 4:1 mixture of hydrogen peroxide (concentration 30%) and sulfuric acid (concentration 96%). Positive photoresist (1813) and developer (MF-322) were bought from Shipley. Metal targets (Cr, Au, and Ag of 99.95% purity) were purchased from Kurt J. Lesker. N-methylpyrrolidone (NMP) was used for lift-off and nitric acid (concentration 70%) was used for dealloying.

Sample preparation: The gold-silver alloy (precursor to np-Au) patterns were created on the glass coverslips with a combination of photolithography, sputter-deposition, and dealloying processes [31]. Briefly, acid-cleaned glass coverslips were coated with 1 μm-thick positive photoresist that was exposed through a transparency mask and developed to form the lift-off layer for subsequent metal deposition. The gold-silver micropatterns were obtained by sequential deposition of 120 nm of chrome (adhesion layer), 80 nm of gold (seed layer), and 500 nm of co-sputtered gold and silver. Following lift-off patterning by immersion in NMP, the samples were dealloyed in 70% nitric acid for 15 minutes at 55 °C to produce the np-Au films. The samples were then rinsed and soaked in DI water for two days to remove any residual nitric acid. CAUTION: Both piranha and nitric acid solutions are highly corrosive and should be handled with care. Please see the Supplementary Information for details of the fabrication process.

Electro-annealing rig: The samples were mounted on a homemade test fixture (Figure S1), consisting of aluminum foil sandwiched between a PCB circuit board and a 1 mm-thick glass slide. Each sample was placed on top of the glass slide and secured with two SEM clips (PELCO SEMClip) that were attached to the circuit board with screws. Constant current was injected into the sample through the clips. We used a switching DC Power supply 1685B (BK Precision) to set constant current and monitor the voltage across the sample. Temperature of the thin film was directly measured by an infrared (IR) thermometer (thermoMETER LS by Micro-Epsilon) stably-positioned over the sample (Figure S-2 in the ESM). The IR spot was positioned at the middle of a trace for unconstricted samples and at the constriction region for the constricted samples. Note that the minimum spot size of the IR thermometer is 1 mm, thus it was not possible to

measure temperature for the constriction sizes smaller than the spot size.

IR thermometers use emissivity to convert detected infrared radiation to temperature. We found that an emissivity value of 0.17 gives reasonably accurate temperature measurements of np-Au surface, covering the entire range of 20 ˚C to 300 ˚C used in this study (Figure S-3b in the ESM). Briefly, the calibration procedure involved the two thermocouples attached onto the surface of hot plate and the IR thermometer positioned above the sample (Figure S-3a in the ESM). Temperatures were recorded every 1 second. Emissivity for np-Au was calibrated by measuring the temperature of the np-Au thin film sample on the hot plate via IR thermometer and comparing it to the temperature readings of both thermocouples. This procedure was repeated for temperature settings on the hot plate from 150 ˚C to 300 ˚C in 25 ˚C increments. Each temperature was held for 2 minutes and a fresh sample was used for each distinct temperature setpoint. In an additional experiment, a fresh sample was placed on hot plate at setpoint of 75 ˚C for 2 minutes; temperature setpoint was incremented in 25 ˚C intervals and held for 2 minutes until 300 ˚C setpoint. After this cycle, the annealed sample was allowed to cool down to room temperature and the calibration procedure was repeated with the same annealed sample to capture possible effects of coarsening on IR-based measurement in comparison to the thermocouple references. For the an emissivity setting of 0.17, between 150 ˚C and 300 ˚C, a measurement error of IR thermometer was less than 7% as compared to the temperature obtained by thermocouples. This error was less than 15% for temperatures between 75 ˚C and 150 ˚C (Figure S-3B in the ESM).

Scanning electron microscopy and morphology analysis: Top and cross-sectional views of the samples were obtained with a scanning electron microscope (FEI Nova NanoSEM430) at 100 kX magnification. The film thickness was determined by examining the cross-sectional images. Highly-coarsened morphologies resulted in few ligaments in a single image at this magnification; therefore for such samples additional images at a lower magnification were obtained. The image analysis results from the 50 kX and 100 kX were pooled together to provide a representative ligament size. SEM images were analyzed using ImageJ (National Institutes of Health shareware). For consistency, automatic thresholding option, which is a variation of IsoData algorithm [32], in ImageJ was used to convert grayscale images to monochrome, where pores are displayed as black and ligaments as white regions. We used MatLab to calculate ligament thickness from the monochrome images. Black and white images were scanned line by line, where ligaments were detected by transition from a black pixel to a white pixel and the number of pixels in each ligament (white pixels) was determined. The total number of pixels for each ligament was converted to a metric value using the SEM scale bars and the median ligament thicknesses were extracted for each image. The effective surface area of the np-Au samples were determined by electrochemical oxide stripping in dilute sulfuric acid as previously described [20].

3. Results and Discussion

3.1 Effect of electro-annealing duration on morphology evolution

We initially studied how pore morphology varies with electro-annealing duration using the unconstricted rectangular np-Au traces (Figure 1A). We evaluated different current settings and

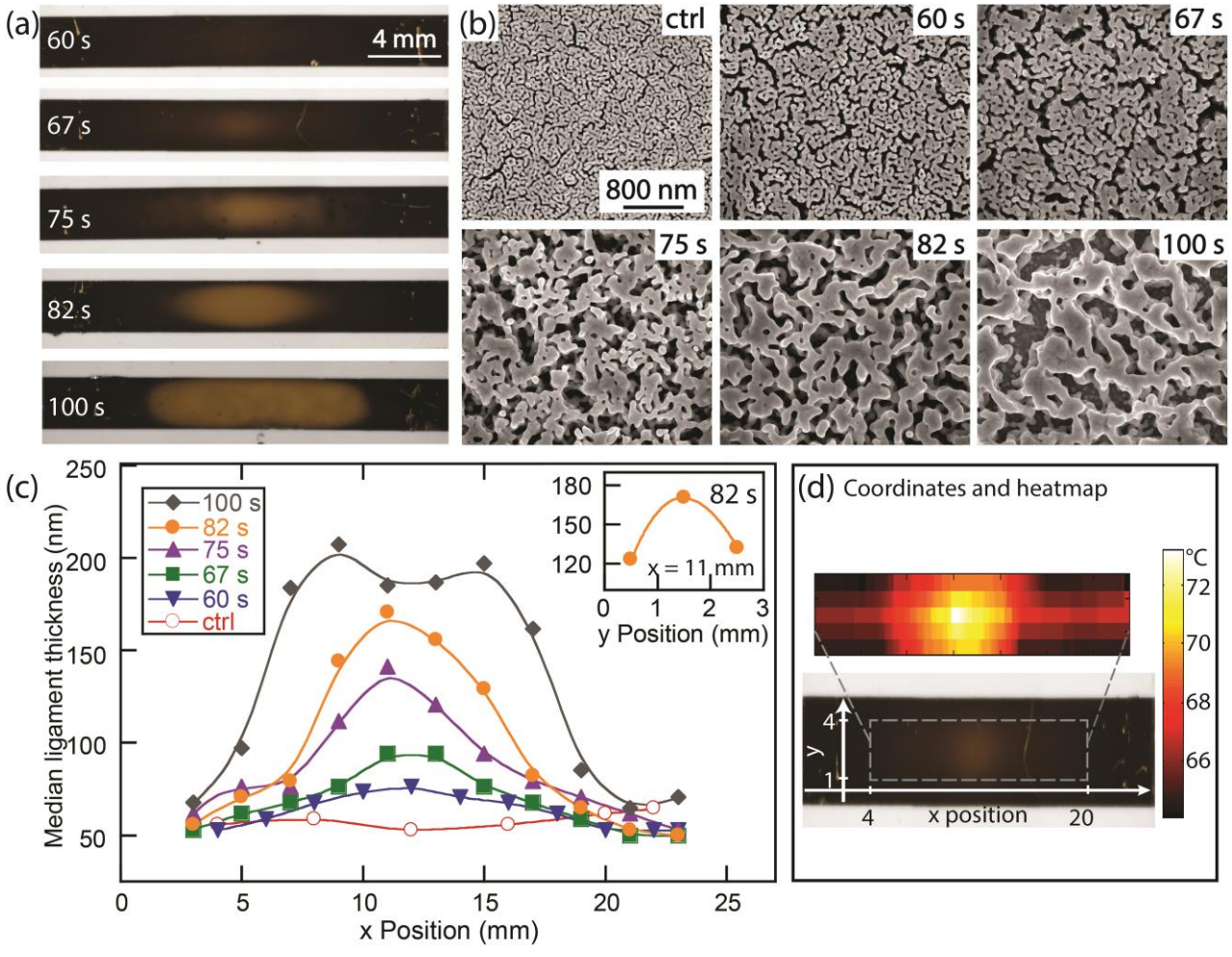

Figure 1. Unconstricted np-Au samples. (a) Photographs of samples that have undergone electro-annealing for 60, 67, 75, 82 and 100 s; and (b) corresponding SEM images taken at the center of each trace. (c) Median ligament thickness vs x-position for each sample. The fitting lines are for visual guides only. Inset shows the ligament thickness versus y-position at x = 11 mm for the 82 s-sample. The extent and span of coarsening increases with electro-annealing duration. (d) Definition of the coordinate nomenclature and the heat map illustrating the temperature distribution over the trace.

determined that 1.5 A offered desirable control over ligament coarsening, as evidenced by color change visible to naked eye. In contrast, lower current settings resulted in negligible coarsening, while higher currents resulted in erratic coarsening. Figure 1a and 1b show photographs and corresponding SEM images of the samples treated at different electro-annealing durations. Figure 2 illustrates cross-sectional SEM images of selected samples that capture the range of morphology evolution shown in Figure 1b. No significant change in pore morphology was observed for treatment durations less than 60 seconds. The color change in the samples treated for longer than 60 seconds indicates higher temperatures in those areas, which is in agreement with coarser pore morphology observed in the SEM images. These high-temperature hot spots generally appear in the middle of the trace, implying that temperature distribution is not uniform over the sample surface (to be discussed below).

To study the hot spot evolution further, we determined median ligament thickness for each sample along the trace length (x-direction) in 2 mm

steps (Figure 1c). The untreated sample had a median ligament thickness of 58 nm. For short treatment durations, the ligament size did not change significantly (i.e., median ligament size for the 60-second treatment is 73 nm). However, the ligament size increased dramatically to approximately 200 nm for the 100 second treatment duration. For this duration, the pore morphology deviated from the characteristic interconnected pore morphology at several locations on the trace and exhibited a more columnar structure uncovering the substrate surface below the porous film (see SEM for 100 s in Figure 1b). The pore morphology through the film thickness remains uniform for moderate electro-annealing (Figure 2b). In the case of heavy-coarsening (i.e., 100 s duration in Figure 1b), the ligaments coalesce into thick columnar structures (Figure 2c) and the number of pores decreases significantly. These cross-sectional images are also consistent with those of typical morphologies obtained by thermal treatment. In addition to the initiation of ligament thickening at the middle of the trace, the coarsening process progresses outwards with increasing treatment duration. This observation is evident for samples treated at 75, 82 and 100 seconds with the latter exhibiting a coarsened morphology in nearly the entire length of the trace (Figure 1a & 1c). We also imaged the 82 seconds sample along the width (y-direction) at the middle of the trace, (inset Figure 1c). In accord with the morphology profile along the trace length, the ligament coarsening is more pronounced in the middle of the trace and drops off slightly near the edges.

The maximum temperature measured at the middle of the trace for the 1.5 A current application for all treatment durations was 140 ± 5 °C. It should be noted that this average value excluded the temperature (172 °C) for the 100 s case because of its atypical morphology (Figure 1b and Figure 2c) and likely effect on electro-annealing behavior.

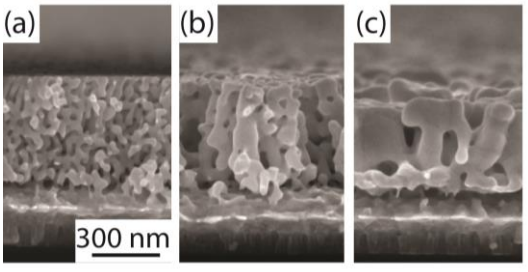

Figure 2. Cross-sectional SEM images of electro-annealed np-Au samples in Figure 1. The images taken at the hotspot correspond to treatment durations of (a) control, (b) 75 s, and (c) 100 s.

Variation of ligament size across the length of the sample suggests that the highest temperature occurs at the middle of the trace. To investigate the temperature distribution over the sample, we measured temperature as a function of position on a 5 mm wide trace by rastering the IR thermometer. We specifically used a wider trace to allow for (i) non-overlapping temperature measurements (note the 1 mm IR spot size); and (ii) a lower maximum temperature at 1.5 A due to a larger trace cross-section and thus less electro-annealing to maintain a stable surface for accurate surface-temperature interrogation. The heat map indeed indicated that the highest temperature coincides with the middle of the trace (Figure 1d), consistent with the ligament coarsening results (Figure 1c). The observed temperature gradient along the trace offers a unique opportunity to create gradually-varying pore morphologies over several millimeters.

The effective surface area of a coating plays an important role for applications ranging from catalysts [16, 17] to biomedical coatings [9-12]. To that end, we tracked changes in surface area at various stages of pore coarsening using electrochemical oxide stripping protocol described previously [20]. While the varying pore morphology of electro-annealed films makes it difficult to obtain an exact surface area that corresponds to a specific pore morphology, we

quantified the surface area of thermally-annealed np-Au films with a uniform pore morphology. These samples were annealed on the hot plate at temperatures that range between 225 °C to 275 °C and capture the range of morphologies obtained via electro-annealing (Figure S-4). The increase in effective surface area with respect to that of a planar gold surface with identical dimensions is referred to as *enhancement factor*, which is expected to decrease with increasing feature size. While the un-annealed np-Au film has a surface area enhancement of 12.8, the 225 °C sample (morphology corresponding to 67 s treatment) had an enhancement factor of 10.7. For the heavily-coarsened morphology (similar to that observed for the 100 s case in Figure 1), the enhancement factor was reduced to 5.1. The drastic change in enhancement factor for samples annealed at temperatures only 25 °C apart highlights the importance of precise control over pore morphology enabled by electro-annealing.

3.2. Effect of geometric constraints on morphology evolution

The spatial location of the hot spot can be controlled by introducing a lithographically-defined geometric constraint in the trace, as shown in the Figure 2a. The dimensions of the constrictions are 2 x 2 mm and overall dimension of the trace is 4 x 24 mm. Basic circuit theory suggests that the geometric constriction causes increased current density in the constriction region and leads to localized coarsening in that area as compared to the rest of the trace. By introducing the constriction at different positions along the trace, we demonstrated that it is possible to control the location of the hot spot and even steer it to multiple and arbitrary locations (Figure 3a).

The SEM images from the middle of constrictions and in the adjacent areas indicate that the constrictions not only allow for controlling the location of the hot spot but also the span of the morphology gradient centered around the hot spot. This finding is illustrated via superimposing the ligament size variations along two different trace geometries (i.e., unconstricted and with one constriction) and aligning the peak locations, as shown in Figure 3c. For the unconstricted case, the coarsened morphology spans approximately 10 mm and shows gradual variation in ligament size with maximum size approaching 210 nm in the middle of the trace. In contrast, for the constricted case coarsening only spans 3 mm with maximum ligament size of approximately 215 nm, a sharp slope in ligament versus distance plot for this sample demonstrates a well-controlled transition between the annealed and unannealed regions of the sample. The ability to precisely control the location and span of pore morphology opens the door to producing high-throughput platforms for studying property-structure relationships.

We hypothesized that having a design with various constriction dimensions on a single trace would create the possibility of engineering a chip with multiple pore morphologies. One such design (labeled as "iv") is shown in Figure 3a. In this configuration, we designed the trace with three progressively decreasing constriction widths (i.e., 2 mm, 1.875 mm, and 1.75 mm). The results indicate that majority of the coarsening occurs in the middle despite the thinnest constriction being on the right. This observation is due to uneven heat dissipation and consequent temperature distribution across the sample as previously discussed (Figure 1d). These results suggest that constriction position and dimensions should be carefully engineered to compensate for higher temperatures at the middle of the trace.

3.3. Branched structures for producing multiple pore morphologies

An alternative design approach with more degrees of freedom is to have multiple traces connected in

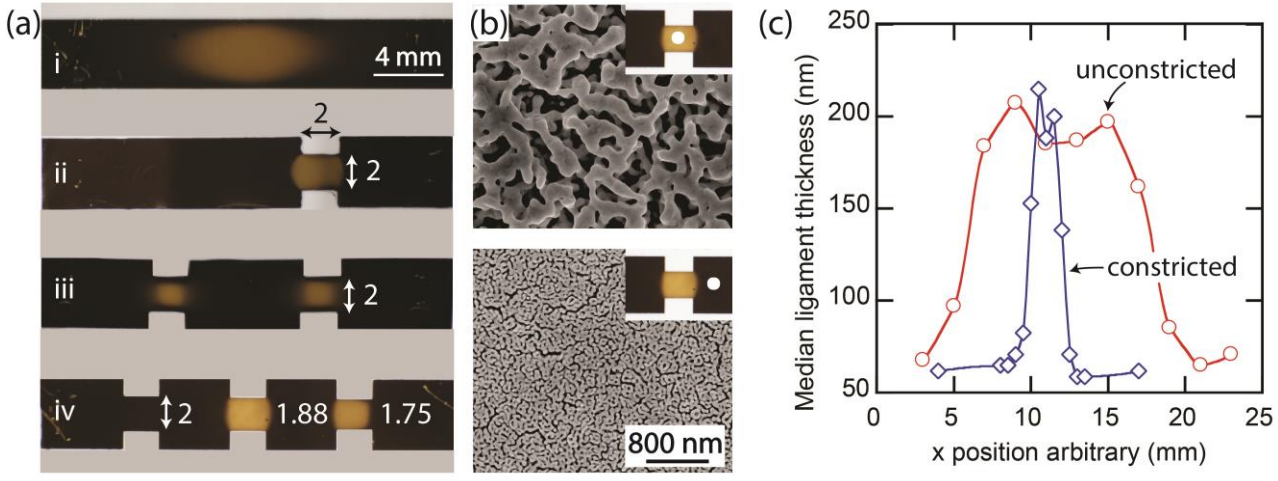

Figure 3. Electro-annealing of samples with geometric constraints. (a) Photos of unconstricted and constricted samples. All constrictions are 2 mm in length (x-direction) and the constriction widths (y-direction) are indicated on the images. (b) SEM images at the constriction and periphery are denoted with the white spots on the photographs in the insets. Trace constrictions allow for programming the location of pore coarsening. (c) Ligament thickness versus position for constricted (2 mm x 2 mm) and unconstricted (annealed for 100 s) samples. The curves were aligned at the peak ligament size for ease of visual comparison

parallel, with constrictions of various dimensions in the middle of each trace (Figure 4a). The major advantage of this approach is that the current density in each branch can be individually controlled not only by the width of the constriction but also by the width of each main trace. This approach can be scaled up to multiple branches informed by electrical circuit (current divider) principles, thus providing a higher degree of control over the resulting pore morphology in each branch. Here, we investigated a basic circuit topology, where each main trace dimension is identical while the constriction dimensions vary. The rationale for this design is that narrower constrictions experience higher Joule heating and enhanced electrically-assisted mechanisms (leading to coarser morphologies) as the current density increases with decreasing constriction width. The constriction lengths were all 1 mm, while the width varied between 0.5 mm to 0.9 mm across the five different traces (Figure 4a).

As a basic circuit analysis would reveal, the current in each branch is largely dictated by the dimensions of the main line, as the constriction is significantly less resistive compared to the main line due to its reduced length. For an applied current of 2 A, we expect the current through each trace to be on the order of 400 mA. Taking constrictions into account, the currents between two successive branches are expected to differ by less than 9 mA. Even though the resistance of the constriction regions increases with temperature, the overall resistance is still largely determined by the main line, as such the current within each branch should not change by more than 7% during electro-annealing. As supported by the SEM images at each constriction (Figure 4b), except for Line 5, a coarser morphology is evident as constrictions become narrower. While Line 5 with the narrowest constriction was expected to have the coarsest morphology due to the highest current density (Figure 4c), the ligament size was between those for Lines 2 and 3 (Figure 4c). This observation is again in agreement with previously discussed uneven heat dissipation and temperature differentials across the sample (Figure 1d). Put another way, the inner lines (2, 3, and 4) run warmer as they receive heat dissipated from the traces around them, while the outer lines (1 and 5)

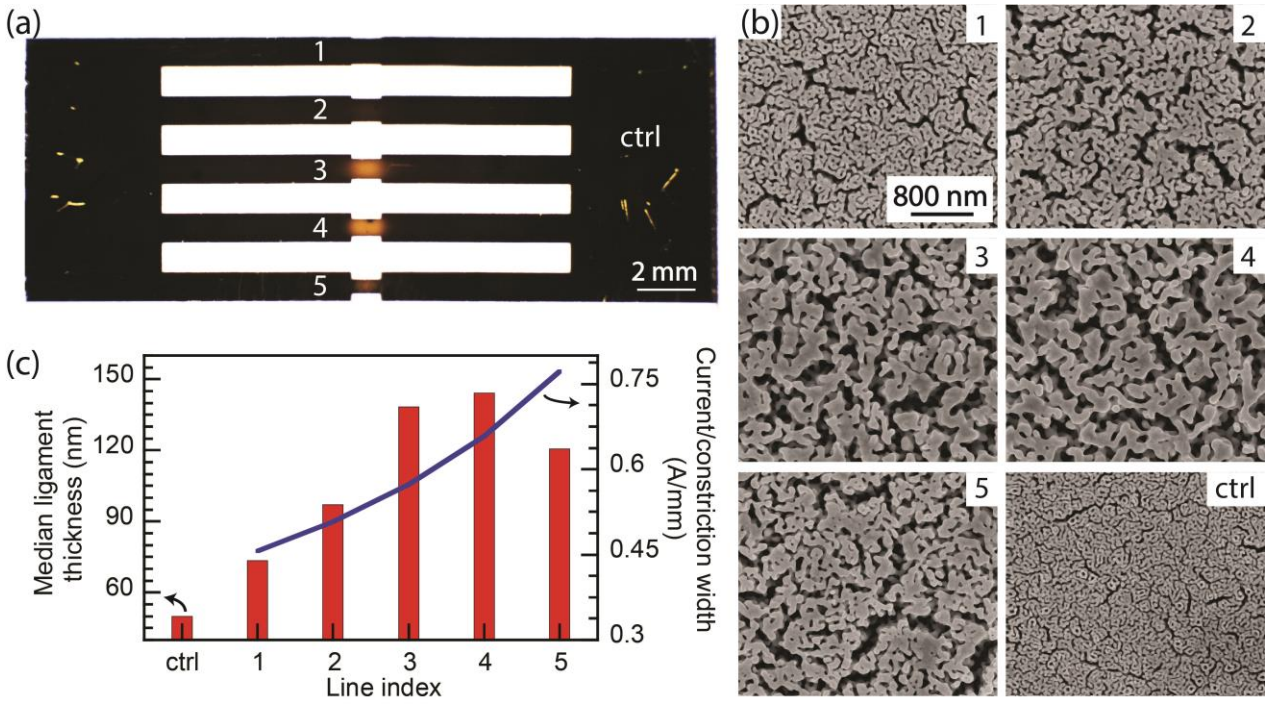

Figure 4. Branched structures for differential electro-annealing. (a) The branched trace design and corresponding SEM images of each constriction in (b). (c) Median ligament thickness and a current-geometry index (i.e., current through each main line divided by individual constriction widths) plotted for each trace. The increasing current-geometry index largely correlates with the extent of ligament coarsening, excluding peripheral lines that are subject to more rapid heat loss.

lose heat faster leading to lower temperatures.

In order to further decouple the effect of varying constriction geometry from the non-uniform temperature distribution, we employed a parallel-trace configuration similar to that used in Figure 4a, except each trace had three identical constrictions. When this trace network was electro-annealed, the coarsening was localized at the constrictions and the influence of temperature distribution (observed in Figure 1d) was superimposed onto the localized coarsening (Figure S-5b in the ESM). More specifically, the constraints at the center were the most coarsened and the coarsening at the constrictions decreased radially outward from the center. This emphasizes that temperature gradient across the sample alone can be utilized for producing varying pore morphologies localized at the constrictions. However, in order to realize a large number of controllable morphologies on a single chip with high spatial and morphological precision, it is necessary to optimize geometric constrictions by incorporating the effect of uneven heat dissipation into the trace circuit design.

3.4. Comparison of electro-annealing and thermal treatment

The effective temperatures measured during electro-annealing were significantly lower than annealing temperatures reported in literature for thermal treatment [23, 29, 31, 33, 34]. Comparison of ligament sizes and temperatures that we obtained during electro-annealing and hot plate calibration also indicated that much higher temperatures were required during thermal annealing to obtain morphologies comparable to those observed with electro-annealing. To confirm this observation, we performed an electro-annealing experiment using an unconstricted 3.5 mm-wide

np-Au trace and measured a maximum temperature of approximately 155 ˚C in the middle of the strip after the color change in the sample (indicative of substantial coarsening). The duration of this treatment was three minutes and the resulting median ligament thickness at the hot spot was 156 nm (Figure 5a left). However, when a np-Au sample (identical to that used for the electro-annealing test) was treated at 155 ˚C (temperature monitored with the same IR thermometer) on the hot plate, there was no color change after 3 minutes of annealing and the measured ligament thickness was 61 nm (Figure 5a right) – similar to that of unannealed samples (58 nm).

Based on hot plate calibration data, it is expected to observe significant coarsening only after 250 ˚C. Indeed, no major coarsening or color change was observed for 3 minute-treatment on the hot plate for temperatures up to 220 ˚C (Figure 5b left). At 250 ˚C on the hot plate, it took 1.5 minutes for np-Au sample to change color. This suggests that in order to obtain comparable ligament sizes between electro-annealing (Figure 5a left) and the hot plate (Figure 5b right), the np-Au temperature on the hot plate should be between 220 ˚C and 250 ˚C, which is nearly 100 ˚C more than effective temperatures recorded for electro-annealing. This hints that temperature alone may not be the only mechanism responsible for ligament coarsening during electro-annealing. The coarsening of np-Au is primarily driven by surface-diffusion-based processes [29, 35]. The surface diffusion coefficient that dictates the rate of the coarsening process follows an Arrhenius relationship [29]:

$$D = D_0 \exp\left(-\frac{E_A}{kT}\right) \qquad (1)$$

where D_0 is the pre-exponential factor, E_A is the activation energy, T is the temperature, and k is the Boltzmann constant.

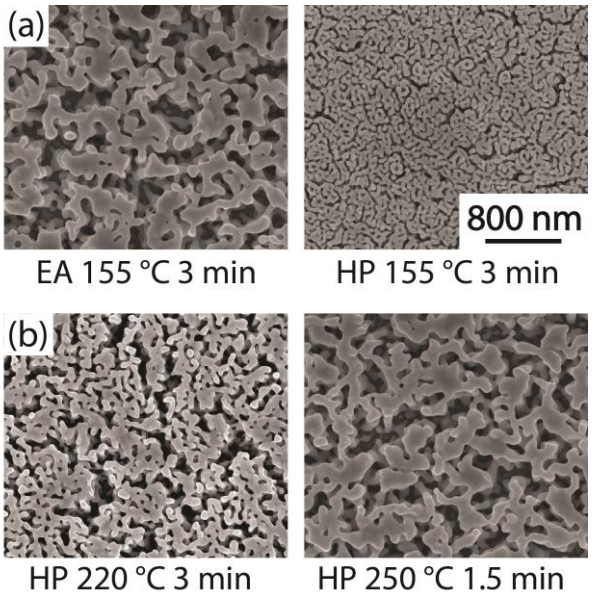

Figure 5. Morphology and temperature comparison for electro-annealing (EA) and hot plate (HP). (a) SEM images of two identical np-Au samples treated at 155 ˚C for 3 minutes via electro-annealing (left) and on hot plate (right). Note that for the same treatment temperature and duration, electro-annealing resulted in significant coarsening while no coarsening was observed for the hot plate case. (b) In order to obtain a similar degree of coarsening with electro-annealing case shown in part (a), a hot plate treatment at 250 ˚C for 1.5 minutes was necessary (right). Note that a 3-minute treatment on hot plate at an intermediate temperature of 220 ˚C did not match the coarsening observed for electro-annealing.

As the equation suggests, the diffusion coefficient, D, increases with temperature, and leads to the experimentally-observed coarsening [31, 33, 34]. For traditional thermal treatment approach, the activation energy necessary to initiate significant surface diffusion is largely provided by thermal energy (kT term) alone. The reduced temperature for the diffusion process, observed during electro-annealing, suggests that additional energy sources complement the thermal energy in initiating the surface diffusion. High current densities have been known to result in electromigration of atoms within wires, which ultimately leads to electromigration-led failure. The

critical current densities for this failure mechanism in gold nanowires with similar characteristic length-scale to that for the np-Au ligaments, has been reported to be on the order of 10^{12} A/m^2. This critical current density is three orders of magnitude higher than the estimated current density per np-Au ligament (on the order of 10^9 A/m^2) for the unconstricted traces investigated here (Figure 1). Also, the SEM images of the electro-annealed samples did not reveal any evidence of electromigration, such as material accumulation downstream of the electron flow direction or nanogap formation in ligaments [36, 37]. It is widely-reported that current flow through small structures (e.g., thin films, nanowires) where mean free path of electrons become comparable to characteristic length-scales of the conductor, the electronic transport is dominated by electron-surface scattering [38, 39]. In the context of np-Au thin films, which can be visualized as a 3D network for nanowires (ligaments), the surface corresponds to the ligament-nanopore interface [38]. Indeed, these scattering events and the resulting energy loss manifest themselves as higher electrical resistance in thin films compared to their bulk counter-part and may be a source of additional energy assisting the coarsening process [40].

For a qualitative discussion of the electro-annealing case, it is helpful to conceptualize the effect of additional energies by modifying the denominator term of the exponential in the Arrhenius equation to $kT + E_{other}$, where E_{other} signifies other putative energies. Some kinetic energy during electro-annealing is dissipated as heat (kT term) which is the temperature rise observed during electro-annealing. The electron collisions during the scattering events would apply a force on the adatoms and the electric field in the ligaments (due to the applied voltage) would exert an additional force on the adatoms. These two forces would constitute E_{other} and translate into increasing the average energy per adatom. Consequently, the surface diffusion of adatoms (thus coarsening) may occur with reduced contribution from the kT term. It is also plausible that the surface diffusion occurs before electromigration, implying that the observed phenomenon may be happening at a transition regime between thermal diffusion and electromigration. The net result is that coarsening occurs at lower temperatures for electro-annealing than for pure thermal treatment. Finally, it should be noted that the complex interplay between these processes that constitute E_{other} are beyond the scope of this work and require further studies, including molecular simulations

4. Conclusion

By taking advantage of the electrical conductivity and morphological plasticity of np-Au, we demonstrated that electro-annealing is a novel and versatile technique to controllably tune pore morphology of np-Au thin films at low temperatures. More specifically, we introduced geometric constrictions into lithographically-patterned np-Au traces and obtained distinct pore morphologies with controllable location and span. This technique is broadly applicable to tuning the nanostructure of other electrically-conductive nanoporous metal systems [6] and amenable to further functionalization via conformal atomic layer deposition of ceramics [41]. We expect this novel approach to be a path to programmable morphology generation using electrical circuit principles and associated CAD tools to design complex trace networks and assist high-throughput screening of structure-property relationships for fundamental and applied studies. We envision that further work in developing a design toolkit that generates optimized trace geometries and electro-annealing parameters will allow for precisely controlling the location and extent of

coarsening. In contrast to traditional thermal coarsening techniques (e.g., furnace, rapid thermal annealing), electro-annealing allows to selectively modify pore morphology simultaneously over different regions on a substrate. When compared to other nascent annealing techniques (e.g., laser sintering [29], the electro-annealing technique does not require sophisticated optical instrumentation, thereby making the method generally available to users with access to simple photolithography and deposition capabilities. While laser micro sintering offers high spatial resolution due to the small laser spot size (few microns), it remains unpractical for creating larger structures (100s of microns to millimeters). In addition, we also observed that temperatures required to obtain significant ligament coarsening during electro-annealing are much lower than temperatures used during traditional thermal annealing, suggesting that other electrically-assisted mechanisms contribute or enhance ligament coarsening during electro-annealing.

Acknowledgements

We gratefully acknowledge the support from UC Lab Fees Research Program Award (12-LR-237197), Research Investments in the Sciences & Engineering (RISE) Award, and UC Davis College of Engineering start-up funds.

Electronic Supplementary Material: Supplementary material further details of the fabrication, IR thermometer calibration, and setup scheme is available in the online version of this article at http://dx.doi.org/10.1007/s12274-***-****-* (automatically inserted by the publisher).

References

[1] Gleiter, H. Nanostructured materials: Basic concepts and microstructure. *Acta Materialia* **2000,** *48*, 1-29.

[2] Suryanarayana, C. Recent developments in nanostructured materials. *Advanced Engineering Materials* **2005,** *7*, 983-992.

[3] Zhang, X.; Xie, H.; Fujii, M.; Ago, H.; Takahashi, K.; Ikuta, T.; Abe, H.; Shimizu, T. Thermal and electrical conductivity of a suspended platinum nanofilm. *Applied Physics Letters* **2005,** *86*, 171912.

[4] Balandin, A. A. Thermal properties of graphene and nanostructured carbon materials. *Nat Mater* **2011,** *10*, 569-581.

[5] Konstantatos, G.; Sargent, E. H. Nanostructured materials for photon detection. *Nat Nano* **2010,** *5*, 391-400.

[6] Seker, E.; Reed, M.; Begley, M. Nanoporous gold: Fabrication, characterization, and applications. *Materials* **2009,** *2*, 2188-2215.

[7] Xiao, X.; Wang, M. e.; Li, H.; Si, P. One-step fabrication of bio-functionalized nanoporous gold/poly(3,4-ethylenedioxythiophene) hybrid electrodes for amperometric glucose sensing. *Talanta* **2013,** *116*, 1054-1059.

[8] Hu, K.; Lan, D.; Li, X.; Zhang, S. Electrochemical DNA biosensor based on nanoporous gold electrode and multifunctional encoded DNA–au bio bar codes. *Analytical Chemistry* **2008,** *80*, 9124-9130.

[9] Seker, E.; Berdichevsky, Y.; Begley, M.; Reed, M.; Staley, K.; Yarmush, M. The fabrication of low-impedance nanoporous gold multiple-electrode arrays for neural electrophysiology studies. *Nanotechnology* **2010,** *21*, 125504.

[10] Seker, E.; Berdichevsky, Y.; Staley, K. J.; Yarmush, M. L. Microfabrication-compatible nanoporous gold foams as biomaterials for drug delivery. *Advanced Healthcare Materials* **2012,** *1*, 172–176.

[11] Tan, Y. H.; Schallom, J. R.; Ganesh, N. V.; Fujikawa, K.; Demchenko, A. V.; Stine, K. J. Characterization of protein immobilization on nanoporous gold using atomic force microscopy

and scanning electron microscopy. *Nanoscale* **2011,** *3*, 3395-3407.

[12] Patel, J.; Radhakrishnan, L.; Zhao, B.; Uppalapati, B.; Daniels, R. C.; Ward, K. R.; Collinson, M. M. Electrochemical properties of nanostructured porous gold electrodes in biofouling solutions. *Analytical chemistry* **2013,** *85*, 11610-11618.

[13] Lang, X.; Hirata, A.; Fujita, T.; Chen, M. Three-dimensional hierarchical nanoporosity for ultrahigh power and excellent cyclability of electrochemical pseudocapacitors. *Advanced Energy Materials* **2014,** *4*, 1301809.

[14] Kucheyev, S.; Hayes, J.; Biener, J.; Huser, T.; Talley, C.; Hamza, A. Surface-enhanced raman scattering on nanoporous au. *Applied Physics Letters* **2006,** *89*, 053102-053104.

[15] Santos, G. M.; Zhao, F.; Zeng, J.; Shih, W.-C. Characterization of nanoporous gold disks for photothermal light harvesting and light-gated molecular release. *Nanoscale* **2014,** *6*, 5718-5724.

[16] Wittstock, A.; Zielasek, V.; Biener, J.; Friend, C. M.; Bäumer, M. Nanoporous gold catalysts for selective gas-phase oxidative coupling of methanol at low temperature. *Science* **2010,** *327*, 319-322.

[17] Xu, C.; Su, J.; Xu, X.; Liu, P.; Zhao, H.; Tian, F.; Ding, Y. Low temperature co oxidation over unsupported nanoporous gold. *Journal of the American Chemical Society* **2006,** *129*, 42-43.

[18] Lee, D.; Wei, X.; Chen, X.; Zhao, M.; Jun, S.; Hone, J.; Herbert, E.; Oliver, W.; Kysar, J. Microfabrication and mechanical properties of nanoporous gold at the nanoscale. *Scripta materialia* **2007,** *56*, 437-440.

[19] Jin, H. J.; Weissmüller, J. A material with electrically tunable strength and flow stress. *Science* **2011,** *332*, 1179-1182.

[20] Kurtulus, O.; Daggumati, P.; Seker, E. Molecular release from patterned nanoporous gold thin films. *Nanoscale* **2014,** *6*, 7062 - 7071.

[21] Senior, N.; Newman, R. Synthesis of tough nanoporous metals by controlled electrolytic dealloying. *Nanotechnology* **2006,** *17*, 2311-2316.

[22] Erlebacher, J. An atomistic description of dealloying. *Journal of the Electrochemical Society* **2004,** *151*, C614-C626.

[23] Hakamada, M.; Mabuchi, M. Thermal coarsening of nanoporous gold: Melting or recrystallization. *Journal of Materials Research* **2009,** *24*, 301-304.

[24] Fujita, T.; Qian, L.-H.; Inoke, K.; Erlebacher, J.; Chen, M.-W. Three-dimensional morphology of nanoporous gold. *Applied Physics Letters* **2008,** *92*, 251902.

[25] Qian, L. H.; Chen, M. W. Ultrafine nanoporous gold by low-temperature dealloying and kinetics of nanopore formation. *Applied Physics Letters* **2007,** *91*, 083105.

[26] Detsi, E.; van de Schootbrugge, M.; Punzhin, S.; Onck, P. R.; De Hosson, J. T. M. On tuning the morphology of nanoporous gold. *Scripta Materialia* **2011,** *64*, 319-322.

[27] Dong, H.; Cao, X. Nanoporous gold thin film: Fabrication, structure evolution, and electrocatalytic activity. *The Journal of Physical Chemistry C* **2008,** *113*, 603-609.

[28] Hakamada, M.; Mabuchi, M. Microstructural evolution in nanoporous gold by thermal and acid treatments. *Materials Letters* **2008,** *62*, 483-486.

[29] Schade, L.; Franzka, S.; Mathieu, M.; Biener, M. M.; Biener, J.; Hartmann, N. Photothermal laser microsintering of nanoporous gold. *Langmuir* **2014,** *30*, 7190-7197.

[30] Klein, R. *Laser welding of plastics*. Wiley: 2011.

[31] Daggumati, P.; Kurtulus, O.; Chapman, C. A. R.; Dimlioglu, D.; Seker, E. Microfabrication of nanoporous gold patterns for cell-material interaction studies. **2013,** e50678.

[32] Sezgin, M.; Sankur, B. Survey over image thresholding techniques and quantitative performance evaluation. *Journal of Electronic Imaging* **2004,** *13*, 146-168.

[33] Hodge, A. M.; Biener, J.; Hayes, J. R.; Bythrow, P. M.; Volkert, C. A.; Hamza, A. V. Scaling equation

for yield strength of nanoporous open-cell foams. *Acta Materialia* **2007,** *55*, 1343-1349.

[34] Li, R.; Sieradzki, K. Ductile-brittle transition in random porous au. *Physical Review Letters* **1992,** *68*, 1168-1171.

[35] Erlebacher, J. Mechanism of coarsening and bubble formation in high-genus nanoporous metals. *Physical Review Letters* **2011,** *106*, 225504.

[36] Trouwborst, M. L.; van der Molen, S. J.; van Wees, B. J. The role of joule heating in the formation of nanogaps by electromigration. *Journal of Applied Physics* **2006,** *99*, 114316.

[37] Hadeed, F. O.; Durkan, C. Controlled fabrication of 1–2nm nanogaps by electromigration in gold and gold-palladium nanowires. *Applied Physics Letters* **2007,** *91*, 123120.

[38] Fujita, T.; Okada, H.; Koyama, K.; Watanabe, K.; Maekawa, S.; Chen, M. W. Unusually small electrical resistance of three-dimensional nanoporous gold in external magnetic fields. *Physical Review Letters* **2008,** *101*, 166601.

[39] Liu, Z.; Searson, P. C. Single nanoporous gold nanowire sensors. *The Journal of Physical Chemistry B* **2006,** *110*, 4318-4322.

[40] Munoz, R. C. Resistivity induced by a rough surface of thin gold films deposited on mica. *J. Mol. Catal. A-Chem.* **2005,** *228*, 163-175.

[41] Biener, M. M.; Biener, J.; Wichmann, A.; Wittstock, A.; Baumann, T. F.; Bäumer, M.; Hamza, A. V. Ald functionalized nanoporous gold: Thermal stability, mechanical properties, and catalytic activity. *Nano Letters* **2011,** *11*, 3085-3090.

Electronic Supplementary Material

Electrically-tunable pore morphology in nanoporous gold thin

Tatiana S. Dorofeeva[1], and Erkin Seker[1,2](✉)

Type author addresses here. The font is Myriad Pro 9. The affiliation should be the institution where the work was conducted. If the present address of an author differs from that at which the work was carried out, please give the present address as well. For example,
[1] Department of Electrical and Computer Engineering, University of California – Davis, Davis, CA 95616, USA

Supporting information to DOI 10.1007/s12274-****-****-* (automatically inserted by the publisher)

Sample Preparation

The glass cover slips used as substrates, on which metal traces are to be patterned, were cleaned by immersion in a piranha solution for 7 minutes, rinsed in deionized (DI) water, and dried under nitrogen flow. In order to micropattern the metal traces, the cover slips were coated with ~1 μm thick positive photoresist (Shipley 1813) followed by a pre-bake for 90 seconds at 115 ˚C on a hot plate. Transparency mask was used for photolithography. Alignment and exposure was performed on Karl Suss mask aligner with exposure duration of 4.5 seconds at 20 mJ. Exposure was followed by a post-bake for 90 seconds at 115 ˚C. The exposed photoresist was developed in MF-322 (Shipley) for 25 seconds with slight manual agitation. The samples were subsequently loaded into a sputtering machine (Kurt J. Lesker) for thin film deposition. Initially, 120 nm of chrome (to promote adhesion between glass and gold) was sputtered at 300 W, followed by 80 nm of seed gold at 400 W, finally 500 nm of silver and gold were co-sputtered at 100 W and 200 W respectively. All depositions were performed under argon atmosphere at 10 mTorr. The lift-off was performed in NMP (N-methylpyrrolidone) by cycles of 10 seconds of sonication followed by a 10 minute pause until all the photoresist was removed. Elemental compositions of the samples were ascertained with energy dispersive X-ray spectroscopy (Oxford INCA Energy-EDS), the resulting gold and silver content of the films was 36% Au and 64% Ag by atomic %. Deposited samples were dealloyed in 70% nitric acid for 15 minutes at 55 ˚C to produce the np-Au films. The dealloying process typically leads to 3-5% residual silver in the final np-Au film. To completely remove traces of nitric acid after the dealloying, samples were rinsed several times and stored in DI water. After 2 days, samples were removed from water, dried with nitrogen gun and stored in ambient conditions until the conducting the electro-annealing experiments.

Measurement Setup

Samples were mounted on the homemade electro-annealing test fixture (Figure S-1), consisting of an aluminum foil sandwiched between a PCB circuit board and a 1 mm-thick glass slide. The sample was placed on top of glass slide and secured with two SEM clips (PELCO SEMClip) which were attached to the circuit board with screws. Constant current was injected into the sample through the clips. We used switching DC

Address correspondence to Erkin Seker, eseker@ucdavis.edu

Power supply 1685B (BK Precision) to set constant current and monitor the voltage across the sample. Temperature was measured by an infrared thermometer (thermoMETER LS by Micro-Epsilon) stably-positioned over the sample (Figure S-2). For the *unconstricted* samples the temperature was measured in the middle of the trace, for the *constricted* samples temperature was measured at the constrictions.

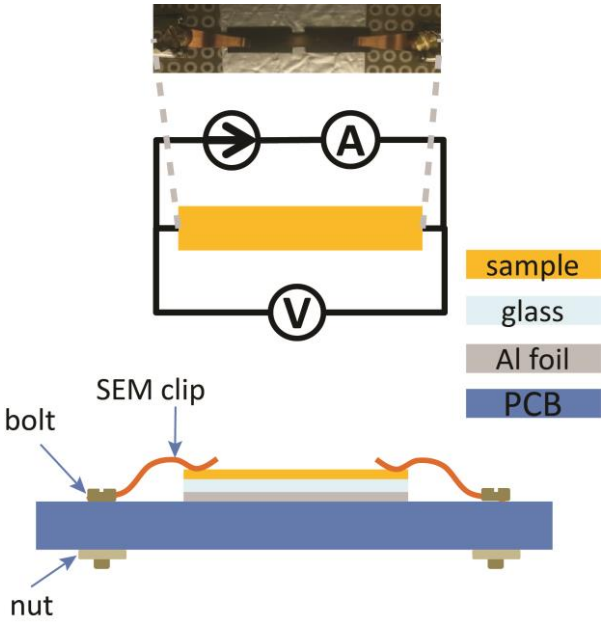

Figure S-1. Electro-annealing test fixture

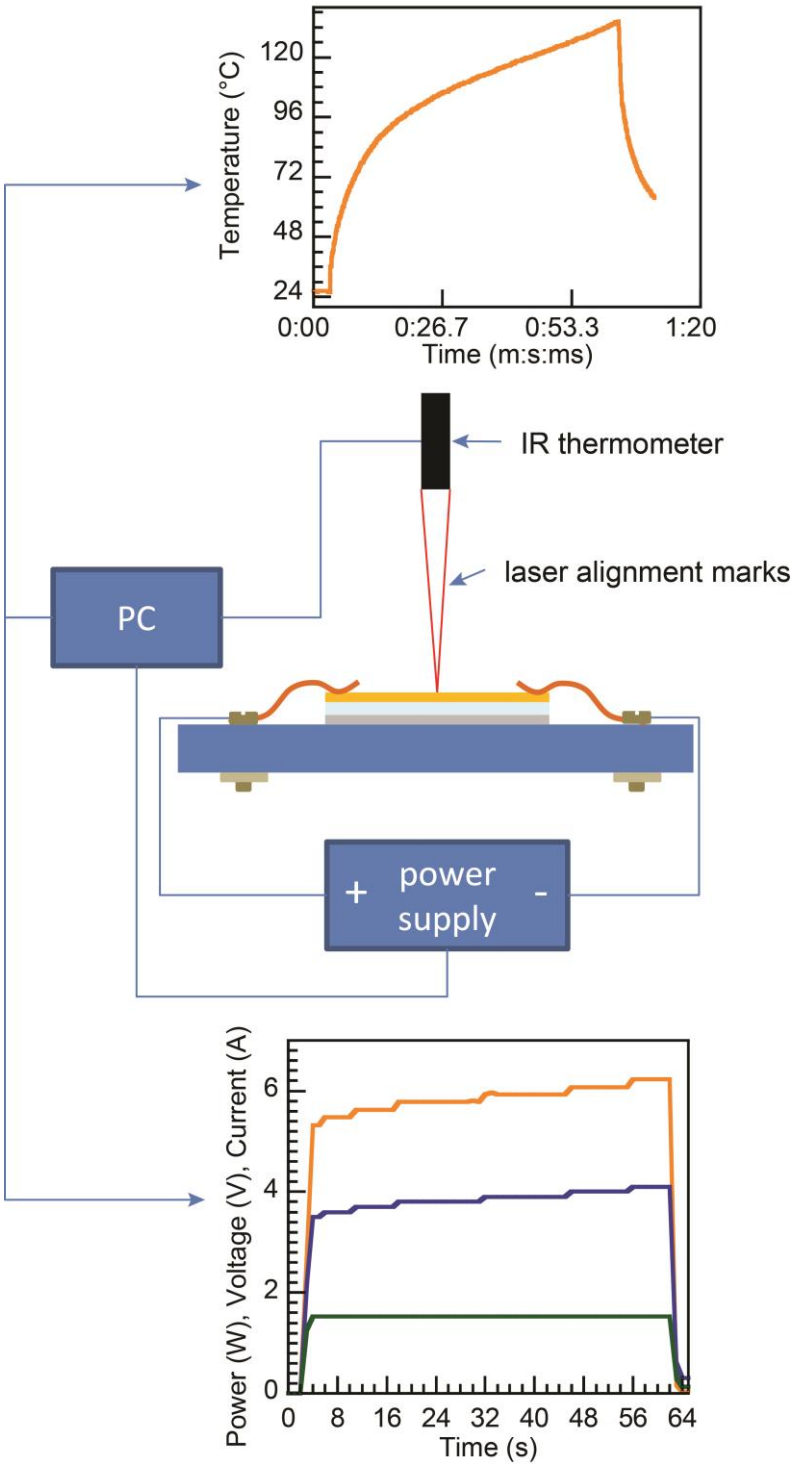

Figure S-2. The setup for electro-annealing is shown as well as sample voltage, current and temperature readings taken during experiments.

Temperature Measurements

Infrared thermometers use emissivity to convert detected infrared radiation to temperature, thus properly choosing the emissivity of np-Au is essential for obtaining proper temperature readings of the np-Au thin films. We utilized two thermocouples (type K), a separate digital thermometer (HH802U by Omega) and a hot plate to calibrate the infrared (IR) thermometer emissivity setting for np-Au. Two thermocouples were attached to the surface of the hot plate using a Kapton tape. One thermocouple was connected to the digital thermometer and second was connected to an auxiliary input port of the IR thermometer. The IR thermometer was positioned above the sample and focused using its laser alignment marks. Both thermometers were connected to a computer through USB cables and the measured temperatures were recorded every 1 second.

The emissivity for np-Au was calibrated by measuring the temperature of the np-Au thin film sample on the hot plate and comparing it to the temperature readings of both thermocouples. IR thermometer calibration in Figure S-3b shows temperature of the hot plate measured using two thermocouples (TC_{Ω} and TC_{IR}) and temperature of np-Au ($TIR_{np\text{-}Au}$) measured by IR thermometer with emissivity set to 0.17. This procedure was repeated for temperature settings on the hot plate from 150 ˚C to 300 ˚C in 25 ˚C increments, each temperature was held for 2 minutes. Fresh np-Au sample was placed on the hot plate before moving on to new setpoint. The calibration indicated that an emissivity (ε) setting of 0.17 gives reasonably accurate temperature measurements of np-Au surface over an entire temperature range 150 ˚C to 300 ˚C. Figure S-3b shows that the temperatures measured by the two thermocouples and temperature of np-Au are all within 10 ˚C of each other in 150 to 300 ˚C.

As an additional experiment to determine if changing morphology during coarsening impacts the accuracy of IR temperature measurement, we performed a similar experiment with only one sample in an expanded lower temperature range from 75 to 300 ˚C. More specifically, a fresh sample was placed on hot plate at setpoint of 75 ˚C for 2 minutes; temperature setpoint was incremented in 25 ˚C intervals and held for 2 minutes until 300 ˚C setpoint. After this cycle, the annealed sample was allowed to cool down to room temperature and the calibration procedure was repeated with the same annealed sample to capture possible effects of coarsening on IR-based measurement in comparison to the thermocouple references. No significant deviations (< 15 ˚C for 75-150 ˚C and < 9 ˚C for 150-300 ˚C) between IR thermometers and thermocouples were observed (Figure S-3b) for the samples covering the entire range of morphologies produced in this study. This suggests that the emissivity of np-Au did not change appreciably at least for the studied morphologies within investigated temperature range.

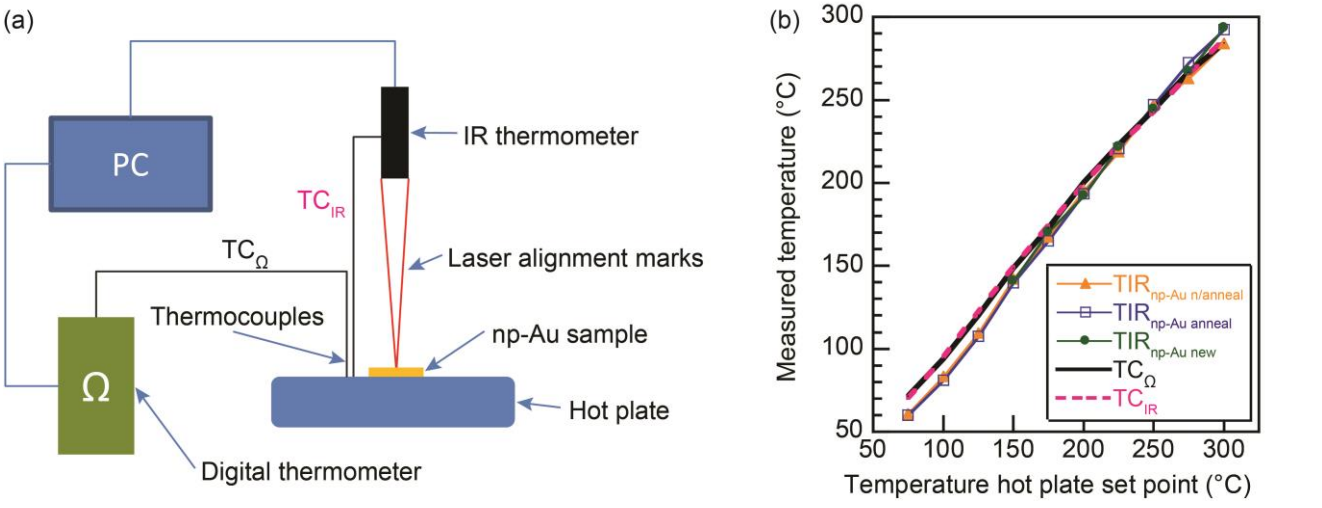

Figure S-3. (a) Temperature calibration setup. (b) The IR thermometer (emissivity set to 0.17) calibration curves with respect to thermocouples for np-Au samples with different degrees of coarsening. The TIR and TC abbreviations in the legend indicate the temperature readings that were obtained by the infrared thermometer and the thermocouples respectively. $TIR_{np\text{-}Au\ n/anneal}$: An unannealed sample was placed on the hot plate and temperature was increased in 25 ℃ increments from 75 ℃ to 300 ℃ while acquiring the sample temperature following two minutes of stabilization after each setpoint. $TIR_{np\text{-}Au\ annealed}$: The same temperature setpoint and acquisition protocol from the previous experiment was used. However, this time an annealed sample (produced in the $TIR_{np\text{-}Au\ n/anneal}$ experiment) was used to evaluate the effect of an already coarsened morphology on IR thermometer readings. $TIR_{np\text{-}Au\ new}$: A fresh unannealed sample was used for each temperature point between 150 ℃ and 300 ℃ in 25 ℃ increments to evaluate the effect of temperature exposure on coarsening at different temperatures. TC_{IR}: Temperature of hot plate directly adjacent to the sample obtained by the thermocouple attached to IR thermometer. TC_{Ω}: Temperature of hot plate directly adjacent to the sample obtained by the thermocouple attached to an additional thermometer.

Surface Enhancement Factor

Electrochemical oxide stripping technique was employed to determine the effective surface areas of np-Au samples. The electrochemical surface characterization (enabled by the electrical conductivity of np-Au) is based on the principle that AuO reduction only happens at the gold surface in contact with the electrolyte and the surface reaction-limited process allows for addressing the entire surface of the np-Au thin film. While the varying pore morphology of electro-annealed films makes it difficult to obtain an exact surface area that corresponds to specific pore morphology, we quantified the surface area of thermally-annealed np-Au films with uniform pore morphology. Fresh np-Au samples were thermally-annealed on the hot plate at 225 °C, 250 °C, and 275 °C for 2 minutes to capture the range of morphologies obtained via electro-annealing. Each np-Au sample with a unique morphology was loaded into a custom-built three-electrode Teflon electrochemical cell with platinum counter electrode and Au/AgCl reference electrode. The np-Au sample was immersed in 0.05 M sulfuric acid and scanned at a rate of 50 mV/s to obtain the corresponding cyclic voltammogram. The total electrical charge under gold oxide reduction peak between potentials of 720 mV and 970 mV was converted to surface area using 450 μC/cm² as the specific charge of a gold surface [1, 2]. The ratio of the effective surface area of the measured sample to that of a planar gold electrode with the same foot print was referred to as "enhancement factor" In Figure S-4 below surface enhancement factor for four different temperature annealing ranges are plotted along with corresponding SEM images illustrating the surface morphology representative for thermal annealing at this temperature, the size of each SEM image is approximately 1x1 μm, we estimate that corresponding JH durations are 67 s, 82 s, and 100 s respectively.

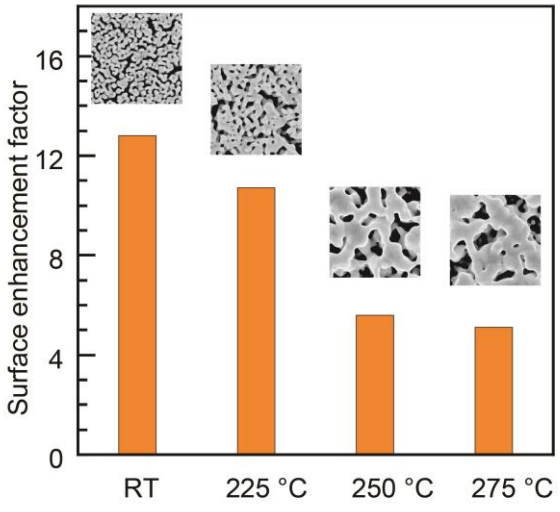

Figure S-4. Area enhancement factor for thermally annealed npAu samples at temperatures of 225 ℃, 250 ℃, and 275 ℃. As guide only, the corresponding electro-annealing durations are approximately 67 s, 82 s, and 100 s (Figure 1). The size of SEM images is 1 μm x1 μm.

Effect of Trace and Electrode Geometry on Temperature Distribution

In order to decouple the effect of varying constriction geometry from the non-uniform temperature distribution, we employed an alternative parallel trace configuration identical to that used in Figure 4a also shown in Figure S-5a below, except each trace has three identical constrictions (Figure S-5b). When this trace network was electro-annealed, the coarsening was localized at the constrictions and as the color change indicates, the influence of temperature distribution (observed in Figures 1d), was superimposed onto the localized coarsening. More specifically, the constraints at the center were the most coarsened and the coarsening at the constrictions decreased radially outward from the center.

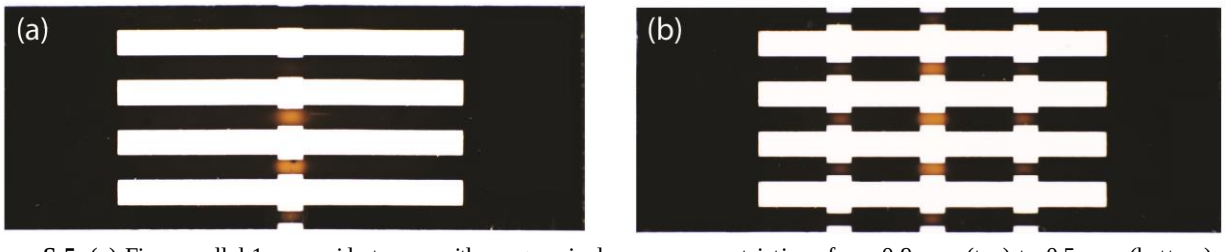

Figure S-5. (a) Five parallel 1 mm-wide traces with progressively narrow constrictions from 0.9 mm (top) to 0.5 mm (bottom). (b) Five parallel 1 mm-wide traces with three 0.5 mm wide constrictions along the length of the trace.

References:

[1] Kurtulus, O.;Daggumati, P.; Seker, E. Molecular Release from Patterned Nanoporous Gold Thin Films. *Nanoscale* **2014**, *6*, 7062 - 7071.

[2] Dong, H.; Cao, X. Nanoporous Gold Thin Film: Fabrication, Structure Evolution, and Electrocatalytic Activity. *The Journal of Physical Chemistry C* **2008**, *113*, 603-609

Address correspondence to Erkin Seker, eseker@ucdavis.edu